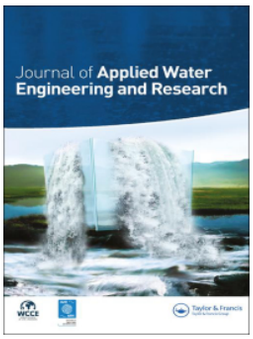

Journal of Applied Water Engineering and Research

ISSN: 2324-9676 (Online) Journal homepage: www.tandfonline.com/journals/tjaw20

Comparing 2D models in simulating suspended sediment processes in vegetated flow

Jiaqi Liu, Alessandra Crosato, Francesco Bregoli & Giulio Calvani

To cite this article: Jiaqi Liu, Alessandra Crosato, Francesco Bregoli & Giulio Calvani (12 Oct 2025): Comparing 2D models in simulating suspended sediment processes in vegetated flow, Journal of Applied Water Engineering and Research, DOI: 10.1080/23249676.2025.2566313

To link to this article: https://doi.org/10.1080/23249676.2025.2566313

JOURNAL OF APPLIED WATER ENGINEERING AND RESEARCH
https://doi.org/10.1080/23249676.2025.2566313

Taylor & Francis
Taylor & Francis Group

Comparing 2D models in simulating suspended sediment processes in vegetated flow

Jiaqi Liu[a,b], Alessandra Crosato[b], Francesco Bregoli[b] and Giulio Calvani[c]

[a]Faculty of Civil Engineering and Geosciences, Delft University of Technology, Delft, the Netherlands; [b]Department of Water Resources and Ecosystems, IHE Delft Institute for Water Education, Delft, the Netherlands; [c]Platform of Hydraulic Constructions (PL-LCH), IIC, School of Architecture, Civil and Environmental Engineering, EPFL, Lausanne, Switzerland

ABSTRACT

Baptist's method, Drag Force and Single-Stem approaches are the commonly used tools implemented in Delft3D to model water and sediment transport processes in vegetated channels. Despite their wide application, the model reliability has seldom been tested against data of controlled flume experiments with solid suspension. Here, we investigate the ability to reproduce suspended sediment transport through emergent vegetation by comparing the results of 2D simulations to existing experimental data. The results show that in low vegetation density, the Baptist and Drag Force approaches are not sensitive enough to density variations. The Single-Stem approach reproduces detailed flow structure and sediment deposition around stems, but its high computational time is a limitation for long-term simulations or dense vegetation. Furthermore, we observed that the simplification of 2D depth-averaged models and the non-equilibrium of sediment transport in both experiments and numerical simulations may also affect the overall performance of the vegetated modelling approaches.

ARTICLE HISTORY
Received 17 January 2025
Accepted 22 September 2025

KEYWORDS
2D numerical modelling; Baptist approach; Delft3D; Drag Force approach; Single-Stem approach; vegetated flow

Introduction

Vegetation plays an important role in aquatic ecosystems, and for this, it is often included in nature-based solutions, considering the morphological developments of alluvial systems and sediment processes. Most studies about the complex interactions between sediment, water flow and vegetation consider sediment transport as bed load (e.g. Yang and Nepf 2018; Bonilla-Porras et al. 2021; Calvani et al. 2023). Although sediment in suspension is common in low-land rivers and is relevant for the transport of pollutants, suspended solids received less attention (Mendez et al. 1999; Fassman 2012; Zhao et al. 2016). To reduce the concentration of pollutants and the turbidity of flowing water, vegetation could be used to filter suspended solids (Srivastava et al. 1996; Monden 2010; Hu et al. 2015; Pierik et al. 2017; Pinho et al. 2018). Emerging vegetation, such as reed, is rather common along lowland river banks and is already used in filtering schemes (Elliott 2000; Deletic 2005; Zong and Nepf 2009; Aiona 2013; Stefanakis 2016; Tseng and Tinoco 2021; Masoud et al. 2022). Flume experiments have been conducted to study suspended sediment deposition and to formulate and validate theoretical models of sediment transport with vegetation (Abt et al. 1994; Sharpe 2003; Zong and Nepf 2011; Borx et al. 2019; Yagci and Strom 2022). The theoretical outcomes have been implemented in numerical tools (Lopez and Garcia 2001; Uittenbogaard 2003; Baptist 2005; Stoesser et al. 2010; Caponi et al. 2022; J. Li et al. 2022). Often, plant stems are represented by rigid cylinders, whereas only a few models account for the characteristics of foliage and stem flexibility (Järvelä 2004; Nepf 2012; Vargas-Luna et al. 2016; Västilä and Järvelä 2017; Li, Xie, et al. 2018; Li, Yang, et al. 2018). Specifically, two approaches are implemented in the open-source Delft 3D suite (Deltares 2018), named Baptist and Drag Force approaches. The presence of vegetation is accounted for as a higher roughness in the momentum equation in the Baptist approach, and an extra drag force of vegetation in the Drag Force approach. However, these two approaches were originally designed for bedload processes, and their reliability has never been tested for suspended sediment transport.

In this work, we investigate the approaches implemented in Delft 3D and their ability to reproduce

CONTACT Jiaqi Liu jliu6@tudelft.nl Faculty of Civil Engineering and Geosciences, Delft University of Technology, Stevinweg 1, 2628 CN, Delft, the Netherlands; Department of Water Resources and Ecosystems, IHE Delft Institute for Water Education, Westvest 7, 2611 AX, Delft, the Netherlands

Supplemental data for this article can be accessed online at https://doi.org/10.1080/23249676.2025.2566313.

the effects of emerging plants on suspended sediment deposition in two-dimensional models. Besides the two most common approaches, the Single-Stem approach, in which each vegetation stem is considered in the numerical grid, is adopted for the sake of comparison.

Two hypotheses are proposed: (1) the most common 2D vegetated flow approaches developed for bedload perform well also with suspended sediment transport under correct calibration;(2) a 2D model considering every single plant stem reproduces the interaction vegetation-sediment-water better than the approaches representing vegetation as uniform extra resistance to the flow.

To test these hypotheses, several numerical simulations are carried out to reproduce flume experiments available in the literature. The performance of the selected approaches is then analysed by comparing both the flow field and sediment deposition results.

Materials and methods

Selected modelling approaches

Baptist's approach (BP)

Baptist's (2005) method, also described in Baptist et al. (2007), allows predicting the effects of vegetation on water flow and sediment transport in one- (1D) and two-dimensional (2D) models through adapted Chézy coefficients.

The approach is based on the subdivision of the total bed shear stress, τ, into bed shear stress, τ_b, and vegetation shear stress, τ_v, assuming dense vegetation, which implies that the flow among the plants can be considered uniform. Plant stems are schematized as rigid cylinders, with diameter D, height h_v and spatial density m. The model can be applied to both submerged and emergent vegetation. With emergent vegetation, the water flows entirely between the plant stems, with flow velocity u_v equal to the depth-averaged flow velocity $\bar{u}$. In this case, the total bed shear stress is calculated as follows:

$$\tau = \tau_b + \tau_v = \frac{\rho g}{C_b^2}\overline{u}^2 + \frac{1}{2}\rho C_D m D h \overline{u}^2 \qquad (1)$$

where g is the gravity acceleration, ρ is the water density, h is the water depth, C_D is the drag coefficient of plants and C_b is the un-vegetated bed roughness coefficient. As a result, the Chézy coefficient, C_r, representing the total hydraulic resistance in the emergent vegetation conditions, is

$$C_r = \sqrt{\frac{1}{\frac{1}{C_b^2} + \frac{C_D m D h}{2g}}} \qquad (2)$$

According to Equation (2), the value of C_r is smaller than C_b, which reflects the higher energy dissipation due to the presence of plants. De facto, the approach corresponds to introducing an additional force in the momentum equations. We remark that in the case of modelling bedload transport, the Chézy coefficient that should be used in the bedload sediment transport formula would be equal to C_b, which contains the critical Shields parameter to determine the initiation of movement of sediment.

Drag Force approach (DF)

In this approach, the effects of vegetation are solely reproduced by adding an extra drag force in the momentum equations. In Delft3D, this is obtained by applying the method of Uittenbogaard (2003), originally designed and implemented for 3D simulations. In 2D depth-averaged (2D) models, the drag force of vegetation per unit area is calculated as

$$F = \frac{1}{2}\rho C_D m D h |\overline{u}| \overline{u} \qquad (3)$$

It is worth observing that, while the Baptist approach regards vegetation as a uniform area with higher flow resistance, the Drag Force approach represents vegetation as an extra drag force in the NavierStokes momentum equation.

Single-Stem approach (SS)

The Single-Stem approach allows reproducing the flow field structure around each stem. This level of detail might be needed to reproduce suspended solids processes, and in particular, sediment deposition, within vegetation.

In this study, the position and size of each stem are obtained by inserting dry points in the computational mesh with computational grid cells that are equal to or smaller than the plant diameter. This means that the marked cells are assumed by the model to be always dry, which is valid only for emergent vegetation. This approach is mainly suitable for sparse vegetation. In Delft3D, this approach does not explicitly account for the drag force exerted by the stems in the momentum equations and, for this reason, the extra energy loss is here obtained by adjusting the eddy viscosity coefficient.

Selected experiments

For testing and comparing the selected numerical approaches, we chose Sharpe's (2003) laboratory experiments based on the study of James et al. (2002). The experiments were conducted in a straight 20 m-long

Table 1. Set-up of the experimental runs carried out by Sharpe (2003) that are used in this study.

Test number	Bed slope (–)	Stem density (stem m^{-2})	Discharge (m^3 s^{-1})	Water depth (m)	Sediment input duration (minutes)
A1.1[C]	0.001873	0	0.00859	0.0617	35
A1.2[V]	0.001873	104	0.00856	0.1303	35
A1.3 [V]	0.001873	194	0.00851	0.1798	35
A1.4 [V]	0.001873	312	0.00859	0.2342	35
A2.1[C]	0.001994	0	0.04431	0.1795	37
A2.2[C]	0.001994	104	0.01295	0.1796	40
A2.3[C]	0.001994	194	0.01092	0.2241	37
A2.4 [C]	0.001994	312	0.0072	0.1918	30
A3.1[C]	0.001994	0	0.02567	0.1244	-

Note: Superscript C: used for calibration; Superscript V: used for validation.

and 0.38 m-wide laboratory flume made of three different sectors. The first two sectors are 5 m long each and have a horizontal bed. The first sector is made of concrete (Manning coefficient, $n = 0.012$ s $m^{-1/3}$ (Chow 1959)) and the second one is made of smooth wood ($n = 0.017$ s $m^{-1/3}$ (Chow 1959)). The third sector is 10 m long and has an adjustable slope and a bed covered by 3M^{TM} Nomad^{TM} Matting to trap deposited sediment and avoid resuspension. This section is also named the test section since all of the measurements are conducted in this part of the flume.

In each test, the flow discharge was kept constant. Steady flow conditions were obtained in the test section by adjusting the weir height at the downstream outlet, then the water depth was measured, and the surface water slope was checked to verify the uniform flow condition. The sediment (with median diameter, D_{50} equal to 0.17 mm) was then fed with a constant rate of 1.73 g s^{-1} via a conveyor belt 0.38 m wide, as a line source at the water surface, 10 m downstream of the flume inlet. The sediment particle Rouse number always fell in the range 0.66–0.96, which ensured particle suspension. Wooden rigid cylinders were used to represent plant stems. The cylinders, with a diameter of 10 mm, were positioned in a staggered pattern with three different densities (104 stem m^{-2}, 194 stem m^{-2} and 312 stem m^{-2}). The sediment feeding duration ranged from 30 to 40 min. After each test, the matting strips covered on the test sections were picked up, then the sediment deposited inside the section of the mat, as well as the flume, was washed out into the separate pans, dried and weighed. For the sake of comparison, unvegetated tests were performed as well. For our investigation, we used 9 of the 12 tests after the analysis of measurement data (Table 1).

Model setup

In this study, both two-dimensional horizontal (2DH) and three-dimensional (3D) hydrodynamic models are employed to investigate flow characteristics. The 2DH models simulate flow by solving the depth-averaged shallow water equations in the horizontal plane, whereas the 3D model accounts for vertical mixing processes through the Reynolds-averaged Navier-Stokes (RANS) equations. Numerical solutions for both modelling approaches are implemented using the Delft3D software suite, which applies a finite difference scheme for spatial and temporal discretization. Commonly, several turbulence closure equations options are available in Delft 3D, i.e. the k-ϵ model, the k-l model or the constant eddy viscosity setting. In this study, we applied the default constant eddy viscosity setting. In both 3D and 2DH models, suspended sediment processes are calculated by applying advection–diffusion equations, with sediment deposition and entrainment formulations as source terms, following the modelling assumption and solution methods approach proposed by Galappatti and Vreugdenhil (1985), then revised by Wang and Ribberink (1986). In Galappatti and Vreugdenhil (1985), the solution of local sediment deposition depends on suspended solids concentration and settling velocity; in Wang and Ribberink (1986) it depends on the difference between bed shear stress and critical bed shear stress for sediment entrainment, as well as on bed erosion speed. The detailed description of the sediment model is reported in the Appendix. For suspended solids, the velocity and water depth of vegetated flow – simulated using the shallow water equations and vegetation-related models – significantly influence sediment movement by determining advection, diffusion and subsequently, erosion and deposition processes. Conversely, sediment transport can also impact the flow by altering the bottom elevation through bed erosion or deposition. These interactions create a coupled system in which water flow and sediment transport continuously influence each other, ultimately shaping the simulation results.

Based on the scale of the model, on the grid size and also on the calibration work of the Single-Stem

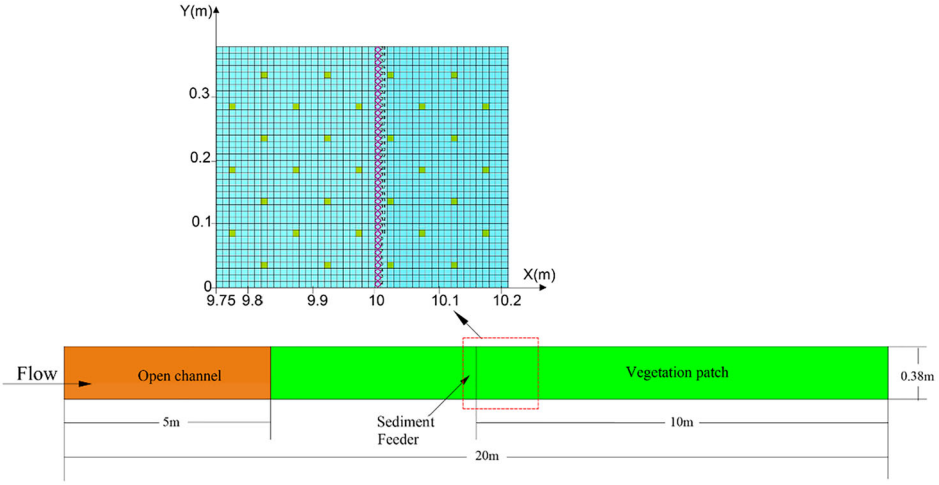

Figure 1. Top view of the flume structure and zoom in on the computational mesh implemented in Delft3D for the Single-Stem approach, indicating the sediment input points (purple diamonds) and the single stems (green squares) with density equal to 194 stems m^{-2}.

approach, the defined constant viscosity and diffusivity value is set to 10^{-4} $m^2 s^{-1}$.

The domain of the models covers the entire experimental flume. It is important to note that the 3M^{TM} Nomad^{TM} Matting used in the experiments by Sharpe (2003) hindered the entrainment of deposited sediment. In the numerical simulations, we simulated the same conditions by imposing an extremely high critical bed shear stress for erosion. For all of the cases, the grid size was set as 0.01 m in both the longitudinal and transversal directions, which is consistent with the vegetation stem diameter of 1 cm, shown in Figure 1. The time step was determined as 0.06 s based on stability criteria, with a maximum Courant number equal to 10 for all the cases, as recommended for the Alternating Direction Implicit (ADI) method used in Delft 3D (Deltares 2018). The three densities in the experiments correspond to stem spacings of 12.7, 9.5 and 7.6 cm, which in the model for the Single-Stem approach become 12, 9 and 7 cm, respectively, corresponding to 109,184 and 296 stems/m^2, respectively. This led to differences of about 5% with respect to the experimental setting, resulting in slightly asymmetric stem distributions in the transverse direction.

The upstream boundary conditions for the flow were discharges, and the downstream boundary conditions were water levels. For sediment, 38 discharge cells were set along the corresponding cross-section to mimic the line sediment source in the experiments (Figure 1). In the numerical simulations, we considered uniform sediment characterized by a single value of settling velocity. The total constant sediment input rate of 1.73 g s^{-1} was equally subdivided among the 38 input cells representing the 0.38 m wide conveyor belt. The resulting sediment concentration was 0.0455 g s^{-1} in each of the 38 input cells. In Delft 3D, continuous suspended sediment input can be realized as a specific concentration in a particular water flow input. So, we set a flow discharge carrying suspended sediment equal to 1 cm^3 s^{-1} with a sediment concentration of 45.53 kg m^{-3} in each discharge cell. This value corresponds to an added flow discharge of 38 cm^3 s^{-1}, which is less than 1% of the total flow discharge.

Model calibration and validation

In this study, the experimental tests A1.1, A2.1 and A3.1, without vegetation, were used to calibrate the roughness coefficient of the bare flume bottom. For the vegetated part, calibration was conducted on tests A2.2, A2.3 and A2.4, with a drag coefficient C_D equal to 1 (as suggested by Vargas-Luna et al. 2016, among others). Manning's coefficient was derived by comparing the computed longitudinal water levels with the experimental ones. This means that its value was derived based on total energy loss, including the loss of energy caused by vegetation. In this case, we cannot refer to 'roughness coefficient' but rather to 'energy loss coefficient'. Baptist's approach required deriving Chézy's coefficient C from Manning's coefficient n by means of the relation $C = n^{-1}R^{1/6}$, where R is the hydraulic radius. The Single-Stem approach required calibrating the horizontal eddy viscosity coefficient.

Validation was based on tests A1.2, A1.3 and A1.4 (Table 1) using the calibrated values of the roughness/energy loss coefficients.

For the transport of suspended solids, we calibrated the value of settling velocity for each approach based

on the experimental tests A2.2, A2.3 and A2.4. The value was obtained by comparing the computed sediment deposition weight against the measured deposition weight along the 6 m length (12 m to 18 m) of the flume.

To evaluate model performance and determine the optimal values of the calibration coefficients, we minimized the Relative Root Mean Square Error (RRMSE) between the experimental and model results of longitudinal velocity and sediment deposition. The RRMSE was calculated as

$$\mathrm{RRMSE} = \frac{\sqrt{\frac{1}{N}\sum_{i=1}^{N}\left(V_m^i - V_c^i\right)^2}}{\frac{1}{N}\sum_{i=1}^{N} V_m^i} \quad (4)$$

where N is the number of values available and V_m and V_c are the modelled and measured values of variable V, respectively. For each calibration test, we selected the value of the coefficient resulting in the lowest RRMSE. More detailed information about calibration and validation is given in the Supplementary Material in Figure S1 and Table S1.

Results of model calibration

As a simplification of the calibration scheme, the Manning coefficient of the unvegetated first half of the flume was set equal to 0.0145 s $m^{-1/3}$, which is the average value of the concrete and wooden bottom mentioned in the experimental setup, corresponding to a Chézy coefficient of 44.43 $m^{1/2}$ s^{-1}. The best performing Manning coefficients for the Nomad covering the test section mat were 0.019, 0.0225 and 0.021 s $m^{-1/3}$ for the tests A1.1, A2.1 and A3.1, respectively, resulting in constant flow depth as in the experiments, with RRMSE smaller than 0.5%. The calibrated value of Manning coefficient was then determined as the averaged value of 0.021 s $m^{-1/3}$, corresponding to the averaged Chézy coefficient of 30.83 $m^{1/2}$ s^{-1}.

For the vegetated area and the Drag Force approach, the optimal Manning coefficient was 0.025 (RRMSE = 0.02%), 0.055 (RRMSE = 0.03%) and 0.08 s $m^{-1/3}$ (RRMSE = 0.02%) for the tests A2.2, A2.3 and A2.4, respectively. For the Baptist approach, the optimal Chézy coefficients were 50 $m^{1/2}$ s^{-1} (RRMSE = 0.01%), 14 $m^{1/2}$ s^{-1} (RRMSE = 0.02%) and 11 $m^{1/2}$ s^{-1} (RRMSE = 0.08%), respectively. These results show that for each vegetation density, both the Baptist and the Drag Force approaches need a different value of roughness coefficient to represent the total energy loss, with higher values for higher vegetation density. For the Drag Force approach, the calibrated Manning coefficient reaches 0.08 s $m^{-1/3}$ in the densest situation. According to the guidelines proposed by Arcement and Schneider (1989), the value of n could reach 0.1 s $m^{-1/3}$ for vegetation, so $n = 0.08$ s $m^{-1/3}$ appears reasonable, corresponding to a low Chézy coefficient in the Baptist approach.

For the Single-Stem approach, the horizontal eddy viscosity was calibrated by comparing the longitudinal water level profiles. The optimal values were $9.5{*}10^{-5}$ m^2 s^{-1} (RRMSE = 0.24%), $1.0{*}10^{-4}$ m^2 s^{-1} (RRMSE = 0.29%) and $7.0{*}10^{-5}$ m^2 s^{-1} (RRMSE = 0.16%) for tests A2.2, A2.3 and A2.4, respectively.

The settling velocity was imposed to fall within the range of 5.69 mm/s (corresponding to the still water settling velocity of a particle having diameter $D_{10} = 0.081$ mm estimated by the Rubey's formula (1933)) and 33.2 mm/s (corresponding to the still water settling velocity of a particle having diameter $D_{90} = 0.25$ mm estimated by the Rubey's formula), with $D_{10}$and D_{90} being the particle diameters below which 10% and 90% of the material's total weight were contained in Sharpe's (2003) experiments, respectively (Table 2). The best performing values of settling velocity increase with vegetation density: for the Baptist and the Drag Force approaches from 7 to 13 mm s^{-1}, for the Single Stem approach from 6 to 12 mm s^{-1}.

Figure 2 shows an example of the measured and computed longitudinal profiles of cumulative deposition weight along the central part of the flume. Sediment accumulates at the upstream section, and the longitudinal profile of sediment deposition becomes steeper with higher settling velocity.

Results of model validation

Hydrodynamic model

Model performance was assessed for the experimental runs A1.2, A1.3 and A1.4 by using the calibrated bed roughness and horizontal eddy viscosity given in Table 2. The RRMSE values between measured and modelled results are overall smaller than 0.1%.

Figure 3 shows the horizontal water level distributions and velocity distribution in the 12–13 m section for test A1.3 obtained with the three different approaches. The Baptist approach and the Drag Force approach result in uniformly distributed flow, whereas the Single-Stem approach results in a flow that passes around the rigid stems, with local differences in water level, higher at the front of the stem and lower downstream of the stems, and also the local difference of velocity distribution between the stems. Similar results were found by Conde-Frias et al. (2022). Seeing plants as distinct obstacles, the Single-Stem approach provides

Table 2. Summary of calibrated coefficients per experimental run and the vegetated modelling approach.

Vegetated modelling approach	Case	Calibrated flow coefficients	RRMSE	Calibrated settling velocity ω_s (mm/s)	RRMSE
Baptist	A2.2	$C_b = 50\ m^{1/2}s^{-1}$	0.01%	7	10.87%
Baptist	A2.3	$C_b = 14\ m^{1/2}s^{-1}$	0.02%	10	4.52%
Baptist	A2.4	$C_b = 11\ m^{1/2}s^{-1}$	0.08%	13	14.76%
Drag Force	A2.2	$n = 0.025\ s\ m^{-1/3}$	0.02%	7	10.83%
Drag Force	A2.3	$n = 0.055\ s\ m^{-1/3}$	0.03%	10	4.52%
Drag Force	A2.4	$n = 0.08\ s\ m^{-1/3}$	0.02%	13	15.35%
Single Stem	A2.2	$\nu_H = 9.50{\cdot}10^{-5}\ m^2s^{-1}$	0.24%	6	7.15%
Single Stem	A2.3	$\nu_H = 1.00{\cdot}10^{-4}\ m^2s^{-1}$	0.29%	9	3.50%
Single Stem	A2.4	$\nu_H = 7.50{\cdot}10^{-5}\ m^2s^{-1}$	0.16%	12	15.23%

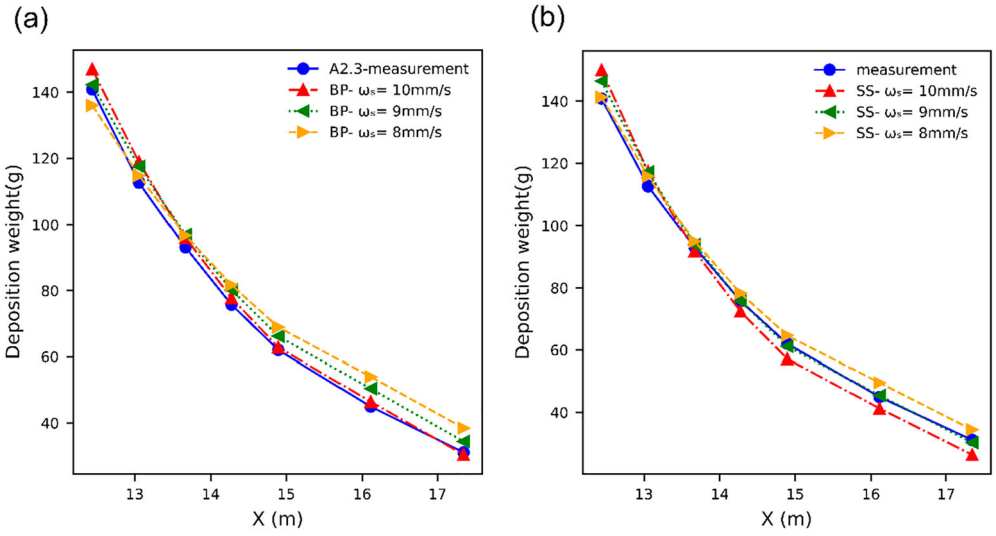

Figure 2. Longitudinal sediment deposition measurements and model output for different values of settling velocity ω_s for the experiment A2.3 using (a) the Baptist approach and (b) the Single-Stem approach.

a more detailed representation of the flow field in a 2D model.

Sediment transport and morphodynamic model

Model results for the tests A1.2, A1.3 and A1.4 are shown in Figure 4. The poorest performance appears in the sparse density case A1.2, where the simulated longitudinal distribution of deposited sediment overestimates the measurements, and the RRMES value is higher than 30%. With the increase in vegetation density, the difference between simulated and measured sediment deposition decreases. The test A1.4 shows the best agreement between measured and simulated deposition, with RRMSE around 10% in three vegetated approaches.

The computed distribution of sediment deposition is shown in Figure 5 for the A1.3 test with 10 mm s^{-1} settling velocity. Both the Baptist and the Drag Force approaches result in uniform sediment deposition in the transversal direction (Figure 5(a)). Instead, sediment deposition is not uniform with the Single-Stem model, with uneven transversal deposition and specifically higher at the left-hand side (Figure 5(b)). This is due to the asymmetric distribution of the stems in the numerical model.

Discussion

Sensitivity of the Baptist and Drag Force approach on vegetation density

The Baptist approach regards vegetation as a uniform area having higher flow resistance, while the Drag Force approach represents vegetation as an extra drag force in the NavierStokes momentum equation. In the 2D model, the two approaches turn out to be very similar. However, the two approaches differ in 3D models because the drag force can vary vertically, whereas Baptist's approach is based on depth-averaged variables. Baptist computes the resistance to the flow exerted by vegetation based on plant characteristics and bed roughness, while the Drag Force approach treats the bottom independently from the plants.

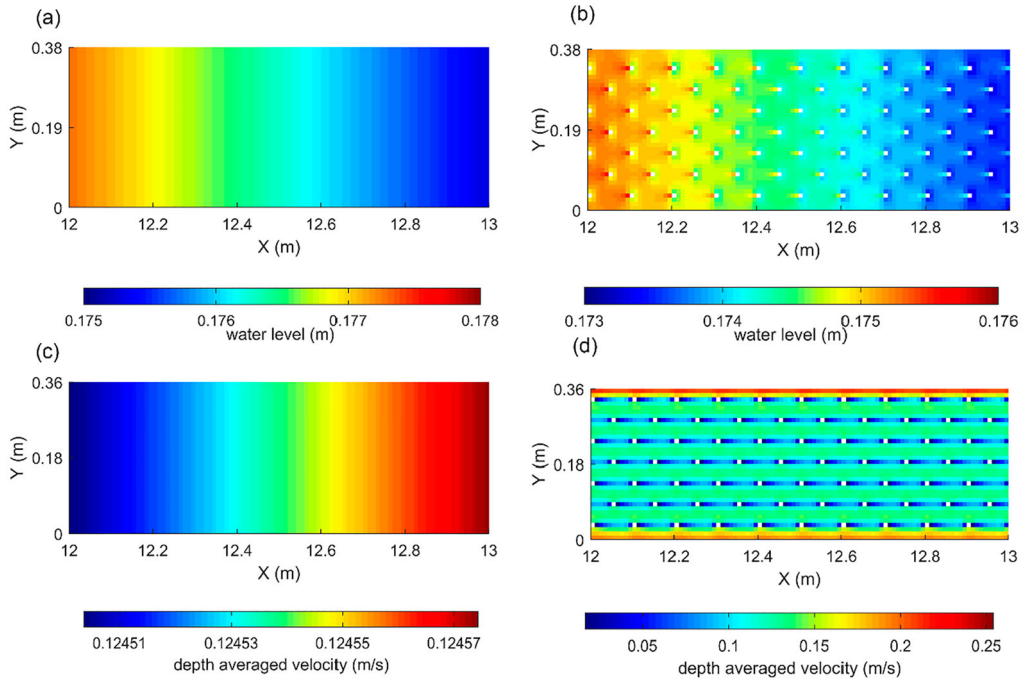

Figure 3. Flow field results in the 12–13 m section for test A1.3: water level distribution of Baptist's and Drag Force approaches (a) and of the Single-Stem approach (b); velocity distribution of the Baptist's and Drag Force approaches (c) and of the Single-Stem approach (d).

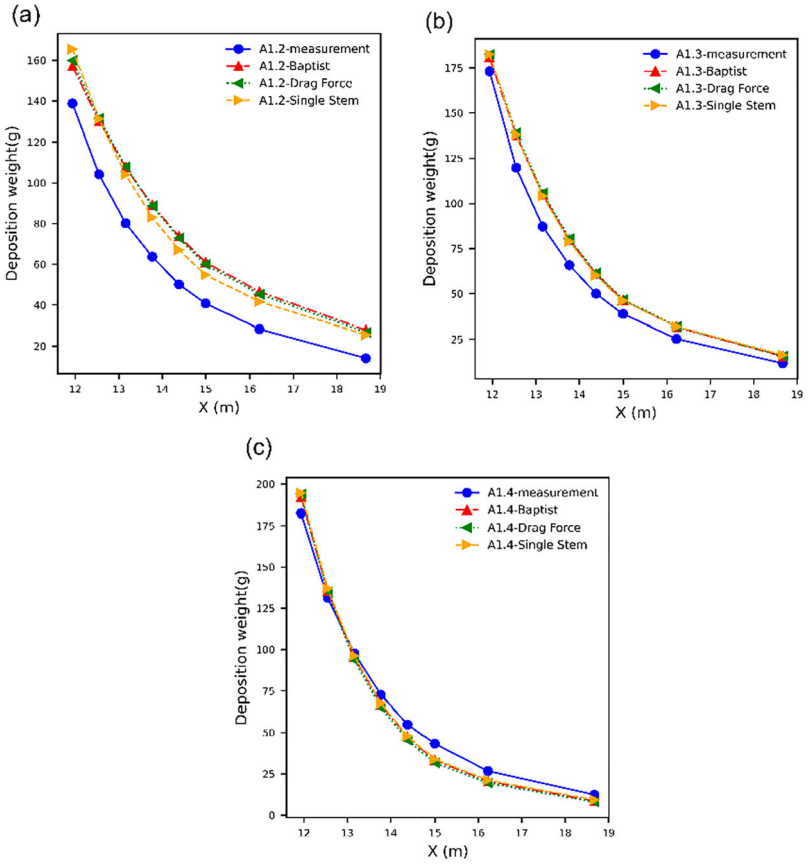

Figure 4. Final longitudinal profile of sediment deposition weight along the channel centre line computed for the validation runs: (a) A1.2, (b) A1.3, (c) A1.4.

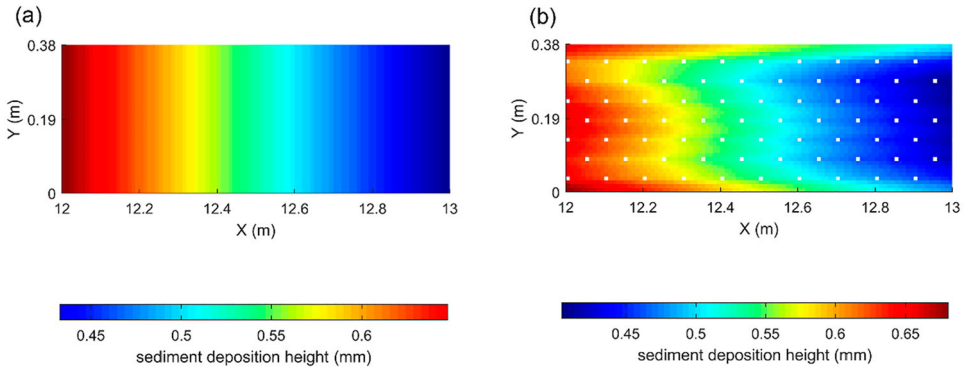

Figure 5. Final sediment deposition distribution for test A1.2 obtained with (a) the Baptist and the Drag Force approaches and (b) the Single-Stem approach.

Some extra computational tests were performed to analyse the sensitivity of the adopted approaches to changes in vegetation density. For this, we reproduced the tests A1.2, A1.3 and A1.4 that have the same boundary conditions, but different vegetation density. The results of the Baptist and Drag Force approaches in 2D are quite similar. Contrary to the experiments, the simulated longitudinal profiles of sediment deposition are the same for all three cases (Figure 6). This indicates that the approaches are not sensitive enough to changes in vegetation density. Baptist's (Figure 6(a)) assumes that the velocity of water flow through vegetation is uniform, which is valid only for dense vegetation. The Drag Force approach (Figure 6(b)) represents the energy dissipation due to the presence of plants only through an added vegetated drag force term. In this way, both the Baptist and the Drag Force approaches need a different roughness coefficient value to represent the total energy loss, with higher values for higher vegetation density. These two approaches do not represent variations of energy dissipations as a function of plant density and would work well only if this is high.

We imposed $C_D = 1$ for both the Baptist and Drag Force approaches. The value of 1 is fairly reasonable when the cylinder Reynolds number (R_d) is larger than 200 and the solid volume fraction φ is smaller than 0.02 (Sonnenwald et al. 2019). This is the case of the simulated experiments, for which $R_d = 1898$, 1282 and 988 and $\varphi = 0.0097$, 0.0174 and 0.0272, for the three vegetation densities, which justifies our choice.

To better represent energy dissipation as a function of vegetation density, we calibrated the roughness coefficient with constant $C_D = 1$. By adopting the different calibrated roughness coefficients in the simulations, we obtained better results, as the RRMSE value is less than 0.2%, shown in Table 2.

The calibrated values increase with vegetation density. Considering that turbulence and energy dissipation normally present a maximum at a certain value of vegetation density and then decrease (e.g. Deitrick et al. 2023; Conde-Frias et al. 2023), the results indicate that the vegetation densities adopted in the experiments are relatively low, i.e. lower than the value corresponding to maximum energy dissipation.

The implication is that for practical applications of the Baptist and Drag Force approaches, to better account for energy dissipation to include also the effects of plants, it is necessary to derive the value of the roughness coefficient as a function of vegetation density.

Effect of physical existence of rigid stem on the flow eddy viscosity and the evaluation of a Single-Stem approach

The Single-Stem approach has the advantage of computing the spatial distribution of flow and sediment deposition around each stem. However, setting up a model representing every single stem is a laborious and time-consuming process, not suitable for large-scale models, since the mesh size should be smaller than or equal to the stem diameter. Moreover, to properly simulate suspended solid processes, the grid size should be about 2–3 times smaller than the sediment deposition length (Facchini 2009). Finally, the Single-Stem approach is very sensitive to the value of eddy viscosity imposed on the model, so this value should be carefully chosen. In this work, the calibrated values of eddy viscosity fell in the range $7.0 \cdot 10^{-5}$ to $1 \cdot 10^{-4}$ m^2 s^{-1}.

Theoretically, in vegetated flows, the eddy viscosity can be calculated as follows:

$$\nu_t = \frac{1}{8} C_t^{-2} C_D D \overline{u} \tag{5}$$

where C_D is the vegetation drag coefficient ($C_D = 1$); C_t is a constant of proportionality, usually considered

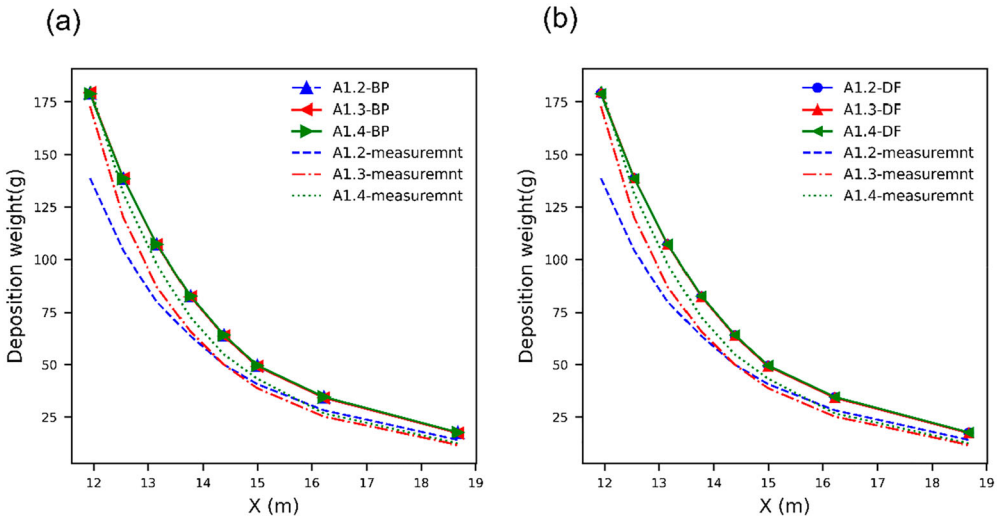

Figure 6. Computed and measured longitudinal profiles of sediment deposition for cases A1.2, A1.3 and A1.4 adopting (a) Baptist's approach and (b) Drag Force approach.

equal to 1, but its value may depend on the shape of the streamwise velocity profile (Kean and Smith 2004).

The theoretical eddy viscosity computed using Equation (5) for the considered tests falls in the range $4.0 \cdot 10^{-3}$ to $2.2 \cdot 10^{-4}$ m^2 s^{-1}, resulting in ratios between calibrated and theoretical values between 0.40 and 0.62 and to values of C_t in the range of 1.55 to 2.27, higher than the theoretical one, but having the same order of magnitude. Based on this, we conclude that the calibrated value of eddy viscosity reasonably falls into the range of applicability. Besides, the horizontal eddy viscosity values obtained for the SS approach differ just a little from the molecular viscosity value; this value may not be high enough to contain the dissipative effects due to the presence of vegetation. This could also be due to the limitation of grid size to make a balance between an enough discretization to get the correct re-attachment length, and a high computational effectiveness. However, the smaller grid size lowers the computational efficiency. To check the model sensitivity to the mesh size, we conducted an extra test on the experimental run A1.3 with a finer mesh of 5 × 5 mm. The spatial distribution of water depth and sediment is shown as Figures S4 and S5 in Supplementary Information. The mean absolute difference and mean absolute relative difference of resulting water depths between the 10 × 10 mm and the 5 × 5 mm mesh size models are reported in Table S2 of Supplementary Information. The test ensures that there are no significant changes in the flow field results, as the mean relative differences relative to the finer mesh are less than 1%. For the morphology, the mean absolute relative difference of deposition weight and the RRMSE value compared with measurement results are also listed in Table S2. The results show that there are also no significant changes in the sediment deposition results as the relative difference is less than 5%. A smaller mesh size means a smaller time step, leading to much longer computational time. In this study, the time required to run the 5 × 5 mm mesh size model is five times that of running the 10 × 10 mm mesh size model when other factors remain constant, not to mention the time spent on the Dry points definition process. Considering the balance between simulated results and computation time, the Single-Stem approach has a big limitation on the scale of the model.

Simplification of the 2DH model in simulating 3D sediment deposition processes

Besides the vegetated modelling approaches, some other important issues can make a significant impact on the simulated results, and one of them is the simplification of the 3D sediment transport process in the 2DH model.

In the experiments, sediment was added to the flume from above, evenly distributed in the transverse direction at a specific cross-section, and the sediment particles reached the bed surface only after a certain travel distance downstream. In 2D models, deposition is calculated as a function of sediment settling velocity times depth-averaged concentration. So, in our 2D computations, sediment is deposited immediately after its release location. At the same time, sediment concentration decreases faster than in the experiments, due to higher loss of sediment in the water

column just after release. Our 2D models predict high deposition upstream of the vegetation patch, where the sediment transport capacity decreases. The reduction of suspended solids concentration in the water column also implies less availability of sediment for deposition within the vegetated patch. Therefore, the results first show an overestimation and then an underestimation of deposition.

To demonstrate this process, a 3D model is established based on the A2.3 Baptist case. The *σ -model* type is set with 4 vertical layers. The calibrated roughness coefficient and 8 mm/s settling velocity are used, and all of the other settings are kept the same as the 2DH model. However, since the parameters in the 3D model are not recalibrated, the results of the 3D model can only be qualitatively analysed and compared with the 2DH results.

Compared with the 2DH model, the 3D results also show a uniform flow distribution along the test section (Figure S3, Supplemental material). As for the suspended sediment transport, the longitudinal deposition height profile from the 9.5 m to 20 m section of the model in 2DH and 3D models is compared in Figure S3b. At the 10 m cross-section (sediment input section), the deposition in the 3D model is lower than the 2D, and the two deposition profiles cross at about 10.5 m. Then, the 3D deposition profile continues to increase until around 11 m and decreases with a steeper slope than the 2DH model. The increasing deposition from 10 m to 11 m in the 3D model shows the impact of the vertical sediment transport process on sediment deposition. The simplification of the vertical sediment transport process in the 2DH model leads to deviations in the sediment deposition results.

It should be emphasized that the problem of not well reproducing deposition profiles in our 2DH models is related to the way sediment is added to the flume in the experiments, i.e. from above. Most real fluvial systems have turbulent flow and well-mixed suspended solids, which would justify the depth-averaging of suspended solids concentration. In general, this problem would appear in the presence of a vertical gradient of sediment concentration. This means that the pros and cons of adopting 2DH models have to be weighed by considering the characteristics of the system to be simulated.

The non-equilibrium sediment transport in both experiments and simulations

Another important issue outside of the vegetated modelling approaches is the non-equilibrium sediment transport process in both experimental work and the simulated study. The presence of aquatic plants is widely regarded as it can reduce the local flow velocity, increase the water depth and promote sediment deposition (Lopez and Garcia 1998) and these quantities are expected to increase with vegetation density (Gran and Paola 2001; Nepf 2012). However, in the experiments, the highest deposition was obtained in the setup without vegetation, the lowest in the sparse density situation (Figure 7). It is difficult to explain the higher deposition in the test without vegetation. We suggest that this was caused by the fact that all systems were still in a morphodynamical transient state at the end of the tests, when measurements occurred, and that those with vegetation were late in their development towards morphodynamical equilibrium compared to the test without vegetation. This is because vegetation lowers the dynamics of the aquatic system, as well as turbulence. In the specific case of the experiment, where sediment input was from above the water surface, it lowered the mixing of sediment, therefore also the near-bed concentration and deposition.

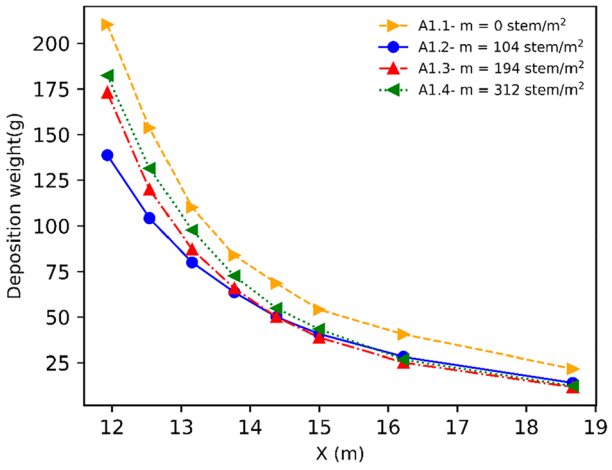

Figure 7. Measurements of sediment deposition weight along the vegetated part of the flume for different vegetation densities *m* (adapted from Sharpe (2003)).

Morphodynamic equilibrium is the morphological state of an aquatic system in which sediment input equals sediment output and bed slope equals water surface slope. The slope develops during the transient phase of the morphological development, through the deposition of sediment upstream (and erosion downstream, if the downstream boundary condition allows). Armanini and Cavedon (2019) and Bonilla-Porras et al. (2021) have shown that higher vegetation density eventually leads to steeper channels, i.e. the equilibrium slope increases with vegetation density. This explains why in the experiments, the lowest deposition occurred

with the sparsest density (see Figure 7). For the case without vegetation, even if the final slope would be smaller than with vegetation, the faster morphological development, due to higher dynamics, results in higher deposition in the upstream part of the test channel, and thus a steeper bed slope, during the transient phase. We can expect this also in Sharp's experiments, but the authors did not provide any considerations on having reached morphodynamic equilibrium or not at the end of their tests (Sharpe 2003). Previous flume experiments dealing with long-term morphodynamics and suspended sediment transport (e.g. Capape et al. 2016) indicate that the final states of Sharpe's tests were most probably at the initial stage of their morphological development, far from equilibrium. To verify this hypothesis, we performed an extended numerical simulation of the A2.4 test with the Single-Stem approach covering over 10 h, a duration much longer than Sharp's experiments. At the end of this long run, the model still shows an ongoing sediment deposition process and zero sediment output, indicating non-equilibrium conditions (Figure S2).

Evaluation of three vegetated modelling approaches in the simulation of suspended sediment transport

The Baptist approach and Drag Force approach, which is generated based on the bed load transport, and in which the vegetation is considered as a uniform block with higher resistance, shows their ability to reproduce the flow field and suspended sediment transport processes with a proper calibration scheme, which verified the first hypothesis in this study. However, it can also be found that, only changing the vegetation parameters and keeping the bottom roughness constant is not enough to get the expected simulated results. The bottom roughness still needs to be calibrated. This leads to a shortcoming of the Baptist and Drag Force approaches: they are not sensitive enough to low vegetation densities.

The Single-Stem approach, which considers the physical presence of rigid stems, can reproduce more detailed local flow field and sediment deposition distribution inside the rigid stems patch than the other two drag force-based modelling approaches, and the second hypothesis in this study is verified. However, the Single-Stem approach has a big limitation in keeping the balance between results accuracy and computational efficiency, especially in dealing with large-scale models. In summary, the advantages and disadvantages of three vegetated modelling approaches are summarized in Table 3.

Table 3. Advantages and disadvantages of the three vegetated modelling approaches in dealing with suspended sediment transport.

Vegetated modelling approaches	Advantages	Disadvantages
Baptist and Drag Force	Wider application scale model; Flexible calibration scheme	Lack of sensitivity to deal with the low vegetation density
Single Stem	The ability to reproduce a more detailed flow field and deposition distribution between vegetation stems	Complex stems setting process; higher requirement on the grid size; higher computational time

Conclusions

The performances of the three widely-used modelling approaches, Baptist, Drag Force and Single Stem, in reproducing the physical processes of suspended sediment in vegetated flows are tested, evaluated and compared at the flume scale. To this effect, we set up 2D models in Delft3D to reproduce measured longitudinal profiles of sediment deposition among vegetation. The results show that the selected 2D vegetated modelling approach developed for the bedload sediment transport can perform well in dealing with the suspended transport under correct calibration. However, both Baptist and Drag Force do not well reproduce the effects of vegetation density on sediment processes, since they show low sensitivity to vegetation density. The Single-Stem approach, which considers the physical existence of vegetation, can reproduce more physical processes between the vegetation-sediment-water system than the approaches that represent vegetation as a uniform extra resistance. However, this advantage is limited by the grid size necessary to get accurate results, and also by the longer time needed to set up and run the model, which is important especially for large-scale applications. Besides the vegetated modelling approach, other issues in the model set-up, such as the simplification of 3D processes in 2D models, also make a relevant impact on the simulated results.

Notation

C_b	bed Chézy coefficient ($m^{1/2}\ s^{-1}$)
C_D	vegetation drag coefficient (-)
C_r	total Chézy coefficient ($m^{1/2}\ s^{-1}$)
C_s	sediment concentration ($kg\ m^{-3}$)
D	stem diameter (m)
g	acceleration due to gravity (m $s^{-}\supset 2$)
h	water depth (m)
h_v	vegetation height (m)
m	cylinder density per unit area (m^{-2})

N	number of the value (-)
n	Manning coefficient (s $m^{-1/3}$)
u_v	vegetated flow velocity (m s^{-1})
$\bar{u}$	depth-averaged velocity (m s^{-1})
V_m and V_c	modelled and measured values of the variable V (-)
x	longitudinal direction (m)
y	lateral direction (m)
z	vertical direction (m)
ρ	water density (kg m^{-3})
τ	bed shear stress (Pa)
ω_s	settling velocity (m s^{-1})
ν_t	eddy viscosity (m^2 s^{-1})
ν_H	horizontal eddy viscosity (m^2 s^{-1})

Acknowledgements

The authors would like to thank Dr Richard Sharpe from Griffith University, Australia, for providing the experimental data and Prof. Wim Uijttewaal of Delft University of Technology, the Netherlands, for fruitful discussions on the eddy viscosity model.

Disclosure statement

No potential conflict of interest was reported by the author(s).

Data availability statement

All data, models and code that support the findings of this study are available from the corresponding author upon reasonable request.

References

Abt SR, Warren PC, Christopher IT. 1994. Sediment deposition and entrapment in vegetated streambeds. J Irrigat Drain Eng. 120(6):1098–1111. https://doi.org/10.1061/(asce)0733-9437(1994)120:6(1098)

Aiona AR. 2013. Can a constructed stormwater facility remove fine particles from urban runoff? University of California Davis.

Arcement GJ, Schneider VR. 1989. Guide for selecting Manning's roughness coefficients for natural channels and flood plains. US Geological Survey Water-Supply Paper 2339. https://doi.org/10.3133/wsp2339

Armanini A, Cavedon V. 2019. Bed-load through emergent vegetation. Adv Water Res. 129:250–259. https://doi.org/10.1016/j.advwatres.2019.05.021

Baptist MJ. 2005. Modelling floodplain biogeomorphology. Delft University of Technology.

Baptist MJet al. 2007. On inducing equations for vegetation resistance. J Hydr Res. 45(4):435–450. https://doi.org/10.1080/00221686.2007.9521778

Bonilla-Porras J, Armanini A, Crosato A. 2021. Extended Einstein's parameters to include vegetation in existing bedload predictors. Adv Water Res. 152:103928. https://doi.org/10.1016/j.advwatres.2021.103928

Borx W, Kaisa V, Juha J. 2019. The interplay between flow field, suspended sediment concentration, and net deposition in a channel with flexible bank vegetation. Water. 11(11):2250. https://doi.org/10.3390/w11112250

Calvani G, Francalanci S, Solari L. 2023. Insights into the dynamics of vegetated alternate bars by means of flume experiments. Water Resour Res. 59(3):e2022WR032536. https://doi.org/10.1029/2022WR032536

Capape S, Martín-Vide JP, Colombo F. 2016. Subaqueous barchans and plane beds from deposition of quartz silt. J Hydr Eng. 142(12). 06016020. https://doi.org/10.1061/(asce)hy.1943-7900.0001212

Caponi F, David V, Davide V. 2022. Baseveg: a python package to model riparian vegetation dynamics coupled with river morphodynamics. SSRN Electron J. 22:101361. https://doi.org/10.2139/ssrn.4167071

Chow VT. 1959. Open channel hydraulics. McGraw-Hill Book Company.

Conde-Frias M, Ghisalberti M, Lowe RJ, Abdolahpour M, Etminan V. 2022. The near-bed flow structure and bed shear stresses within emergent vegetation canopies. Water Resour Res. 59(4). e2022WR032499. https://doi.org/10.1029/2022WR032499

Conde-Frias M, Ghisalberti M, Lowe RJ, Abdolahpour M, Etminan V. 2023. The near-bed flow structure and bed shear stresses within emergent vegetation. Water Resour Res. 59(4). e2022WR032499. https://doi.org/10.1029/2022WR032499

Deitrick AR, Hovendon EH, Ralston DK, Nepf H. 2023. The influence of vegetation-generated turbulence on deposition in emergent canopies. Front Marine Sci. 10:1–10. https://doi.org/10.3389/fmars.2023.1266241

Deletic A. 2005. Sediment transport in urban runoff over grassed areas. J Hydrol. 301(1–4):108–122. https://doi.org/10.1016/j.jhydrol.2004.06.023

Deltares. 2018. 3D/2D modelling suite for integral water solutions: hydro-morphodynamics. Delft.

Elliott AH. 2000. Settling of fine sediment in a channel with emergent vegetation. J Hydr Eng. 126(8):570–577. https://doi.org/10.1061/(ASCE)0733-9429(2000)126:8(570)

Facchini E. 2009. Morphological aspects of cyclic rejuvenation of the Ewijkse Plaat, the Netherlands. IHE Delft Institute for Water Education.

Fassman E. 2012. Stormwater BMP treatment performance variability for sediment and heavy metals. Separat Purif Technol. 84:95–103. https://doi.org/10.1016/j.seppur.2011.06.033

Galappatti G, Vreugdenhil CB. 1985. A depth-integrated model for suspended sediment transport. J Hydr Res. 23(4):359–377. https://doi.org/10.1080/00221688509499345

Gran K, Paola C. 2001. Riparian vegetation controls on braided stream dynamics. Water Resour. Res.. 37(12):3275–3283. https://doi.org/10.1029/2000WR000203

Hu K, Qin C, Wang H. 2015. A numerical study of vegetation impact on reducing storm surge by wetlands in a semi-enclosed estuary. Coast Eng. 95:66–76. https://doi.org/10.1016/j.coastaleng.2014.09.008

James CS, Birkhead AL, Jordanova AA, Kostchy KA. 2002. Interaction of reeds, hydraulics and river morphology. Johannesburg. https://doi.org/10.1016/j.coastaleng.2014.09.008

Järvelä J. 2004. Determination of flow resistance caused by non-submerged woody vegetation. Int J River Basin Manag. 2(1):61–70. https://doi.org/10.1080/15715124.2004.9635222

Kean JW, Smith JD. 2004. Flow and boundary shear stress in channels with woody bank vegetation. In: Bennett SJ, Simon A, editors. Riparian vegetation and fluvial geomorphology. American Geophysical Union. p 237–265. https://doi.org/10.1029/008WSA17

Li D, Yang Z, Sun Z, Huai W, Liu J. 2018. Theoretical model of suspended sediment concentration in a flow with submerged vegetation. Water. 10(11):1656. https://doi.org/10.3390/w10111656

Li Jet al. 2022. Effects of vegetation patch patterns on channel morphology: a numerical study. J Geophys Res Earth Surf. 127(5):1–20. https://doi.org/10.1029/2021JF006529

Li Y, Xie L, Su T. 2018. Resistance of open-channel flow under the effect of bending deformation of submerged flexible vegetation. J Hydr Eng. 144(3). 04017072. https://doi.org/10.1061/(asce)hy.1943-7900.0001419

Lopez F, Garcia M. 1998. Open-channel flow through simulated vegetation: suspended sediment transport modeling. Water Resour Res. 34(9):2341–2352. https://doi.org/10.1029/98WR01922

Lopez F, Garcia M. 2001. Mean flow and turbulence structure of open-channel flow through nonemergent vegetation. J Hydr Eng. 127:392–402. https://doi.org/10.1061/(ASCE)0733-9429(2001)127:5(392)

Masoud A, Alfarra A, Sorlini S. 2022. Constructed wetlands as a solution for sustainable sanitation: a comprehensive review on integrating climate change resilience and circular economy. Water. 14(20):1–16. https://doi.org/10.3390/w14203232

Mendez A, Dillaha TA, Mostaghimi S. 1999. Sediment and nitrogen transport in grass filter strips. J Am Water Resour Assoc. 35(4):867–875. https://doi.org/10.1111/j.1752-1688.1999.tb04180.x

Monden M. 2010. Modeling the interaction between morphodynamics and vegetation in the Nisqually River Estuary. Delft University of Technology.

Nepf HM. 2012. Hydrodynamics of vegetated channels. J Hydr Res. 50(3):262–279. https://doi.org/10.1080/00221686.2012.696559

Pierik HJ, Stouthamer E, Cohen KM. 2017. Natural levee evolution in the Rhine-Meuse Delta, the Netherlands, during the first millennium CE. Geomorphology. 295(7):215–234. https://doi.org/10.1016/j.geomorph.2017.07.003

Pinho Jet al. 2018. Application of Delft3d for designing and assessing new solutions to improve sediment input to an erosion prone coast. EPiC Ser Eng. 3:1664–1655. https://doi.org/10.29007/lqms

Rubey WW. 1933. Settling velocities of gravel, sand, and silt particles. Am J Sci. 25(148):325–338.

Sharpe R. 2003. Suspended sediment transport through non-submerged reeds. University of the Witwatersrand.

Sonnenwald F, Guymer I, Stovin V. 2019. A CFD-based mixing model for vegetated flows. Water Resources Research . 55:2322–2347. https://doi.org/10.1029/2018WR023628

Srivastava P, Edwards DR, Daniel TC, Moore PA, Costello TA. 1996. Performance of vegetative filter strips with varying pollutant source and filter strip lengths. Am Soc Agricult Eng. 39(6):2231–2239. https://doi.org/10.13031/2013.27730

Stefanakis A. I. 2016. Constructed wetlands: description and benefits of an eco-tech water treatment system. In: Impact of water pollution on human health and environmental sustainability. IGI Global Scientific Publishing; p. 281–303.

Stoesser T, Kim SJ, Diplas P. 2010. Turbulent flow through idealized emergent vegetation. J Hydr Eng. 136(12):1003–1017. https://doi.org/10.1061/(asce)hy.1943-7900.0000153

Tseng CY, Tinoco RO. 2021. A two-layer turbulence-based model to predict suspended sediment concentration in flows with aquatic vegetation. Geophys Res Lett. 48(3):1–14. https://doi.org/10.1029/2020GL091255

Uittenbogaard R. 2003. Modelling turbulence in vegetated aquatic flows. In: International workshop on RIParian FORest vegetated channels: hydraulic, morphological and ecological aspects. 20–22.

Vargas-Luna A, Crosato A, Calvani G, Uijttewaal WSJ. 2016. Representing plants as rigid cylinders in experiments and models. Adv Water Resour. 93:205–222. https://doi.org/10.1016/j.advwatres.2015.10.004

Västilä K, Järvelä J. 2017. Characterizing natural riparian vegetation for modeling of flow and suspended sediment transport. J Soils Sedim. 18(10):3114–3130. https://doi.org/10.1007/s11368-017-1776-3

Wang ZB, Ribberink JS. 1986. The validity of a depth-integrated model for suspended sediment transport. J Hydr Res. 24(1):53–67. https://doi.org/10.1080/00221688609499332

Yagci O, Strom K. 2022. Reach-scale experiments on deposition process in vegetated channel: suspended sediment capturing ability and backwater effect of instream plants. J Hydrol. 608(11):127612. https://doi.org/10.1016/j.jhydrol.2022.127612

Yang JQ, Nepf HM. 2018. A turbulence-based bed-load transport model for bare and vegetated channels. Geophys Res Lett. 45(19):10,428–10,436. https://doi.org/10.1029/2018GL079319

Zhao C, Jian E, Meng J, Wang F, Zhang T. 2016. Sediment deposition and overland flow hydraulics in simulated vegetative filter strips under varying vegetation covers. Hydrol Process. 30(2):163–175. https://doi.org/10.1002/hyp.10556

Zong L, Nepf H. 2009. Flow and deposition in and around a finite patch of vegetation. Geomorphology. 116(3–4):363–372. https://doi.org/10.1016/j.geomorph.2009.11.020

Zong L, Nepf H. 2011. Spatial distribution of deposition within a patch of vegetation. Water Resour Res. 47(3):1–12. https://doi.org/10.1029/2010WR009516

Appendix

Sediment transport model

In Delft 3D, the suspended sediment can be calculated by the advection-diffusion (AD) equation. In this study, the 2D version AD equation is applied, in which the sediment concentration represents the depth-averaged value:

$$\frac{\partial C_s}{\partial t} + u_x \frac{\partial C_s}{\partial x} + u_y \frac{\partial C_s}{\partial y} = \frac{\partial}{\partial x}\left(\varepsilon_x \frac{\partial C_s}{\partial x}\right) + \frac{\partial}{\partial y}\left(\varepsilon_y \frac{\partial C_s}{\partial y}\right) + D - E$$

where x is the longitudinal coordinate; y is the transverse coordinate. Cs is the concentration; u_x, u_y are flow velocity in the x–y direction; ε_x, ε_y are eddy diffusivities of sediment in the x–y–z direction.

For finer sediment particles, the erosion E and deposition D of particles is calculated as the Partheniades-Krone formulations in Delft 3D, which are

$$E = MS(\tau_{cw}, \tau_{cr,e})$$

$$D = \omega_s c S(\tau_{cw}, \tau_{cr,d})$$

where M is the erosion parameter, which is set as 1 in the model; c is the average sediment concentration in the near-bottom computational layer, which is equal to the depth-averaged concentration in 2D models. $S(\tau_{cw}, \tau_{cr,e})$ and $S(\tau_{cw}, \tau_{cr,d})$ are the erosion and the deposition step functions, respectively, which depend on the maximum bed shear stress due to waves and current τ_{cw}, as well as on the critical bed shear stress for erosion and deposition $\tau_{cr,e}$ and $\tau_{cr,d}$ (to be defined), respectively:

$$S(\tau_{cw}, \tau_{cr,e}) = \begin{cases} \left(\frac{\tau_{cw}}{\tau_{cr,e}} - 1\right), & \tau_{cw} \geq \tau_{cr,e} \\ 0, \tau_{cw} \leq \tau_{cr,e} \end{cases}$$

$$S(\tau_{cw}, \tau_{cr,d}) = \begin{cases} \left(\frac{\tau_{cw}}{\tau_{cr,d}} - 1\right), & \tau_{cw} \leq \tau_{cr,d} \\ 0, \tau_{cw} \geq \tau_{cr,d} \end{cases}$$

Since a Nomad mat covers the test section to trap the deposited sediment and avoid resuspension, both the critical deposition and erosion shear stress are set to the maximum value in Delft 3D, which are 1000 and 100 Nm^{-2}, respectively, to make sure particles are allowed by the model to deposit but cannot be resuspended.

The settling velocity is firstly calculated with Rubey's formula and then calibrated:

$$\omega_s = \sqrt{\frac{2\Delta g D}{3} + \frac{36\nu^2}{D^2}} - \frac{6\nu}{D}$$

where Δ is the relative sediment density $(\rho_s - \rho) / \rho$, where $\rho_s$is the sediment density and ρ is the water density; D is the sediment diameter; ν is the kinematic viscosity of water and g is the acceleration due to gravity. However, the settling velocity is considered a calibrated parameter. In Delft 3D, both horizontal eddy viscosity and eddy diffusivity could be set as calibrated parameters. The horizontal eddy diffusivity is set as the same value as horizontal eddy viscosity so that the turbulent Schmidt number, which is the ratio of these two parameters, becomes equal to 1.